Heat-Treated Non-precious Metal Catalysts for Oxygen Reduction

Hoon Chung, Gang Wu, Drew Higgins, Pouyan Zamani, Zhongwei Chen and Piotr Zelenay

1 Introduction

1.1 Polymer Electrolyte Fuel Cells—The Cathode Challenge

Polymer electrolyte fuel cells (PEFCs) are touted as a green alternative to the internal combustion engine, yet commercial penetration of PEFCs into the automotive sector remains hindered by cost and durability issues. Under projected conditions of mass production, almost half of the overall fuel cell stack cost is due to the expensive platinum-based catalysts [1]. Current cost targets are unattainable unless the extensive reliance on this precious metal is alleviated. This can only be accomplished by developing alternative cathode catalysts for the oxygen reduction reaction (ORR). Research on new platinum catalyst supports or nanostructured platinum alloys to increase ORR activity on a precious metal mass basis have been largely successful [2–6]. This approach is not ideal, however, due to the volatile pricing and geopolitical instabilities that can likely affect the supply of platinum. For these reasons, the development of entirely non-platinum group metal (non-PGM) catalysts for the oxygen reduction reaction (ORR) is highly desirable [7–9].

H. Chung · P. Zelenay (✉)
Materials Physics and Applications Division, Los Alamos National Laboratory, Los Alamos, New Mexico 87545, USA
e-mail: zelenay@lanl.gov

G. Wu
Department of Chemical and Biological Engineering, University at Buffalo, SUNY, Buffalo, New York 14260, USA

D. Higgins · P. Zamani · Z. Chen
Department of Chemical Engineering, University of Waterloo, Waterloo, Ontario N2L 3G1, Canada

J.H. Zagal and F. Bedioui (eds.), *Electrochemistry of N4 Macrocyclic Metal Complexes*, DOI 10.1007/978-3-319-31172-2_2

Several different non-PGM catalysts have been investigated in the scientific community. Among them, the most promising systems in terms of activity and stability are made by heat-treating a mixture of transition metal nitrogen, and carbon species (M–N–C) at temperatures in excess of 700 °C [10]. Different synthesis approaches, precursor selection, and fabrication parameters are known to result in catalyst variations, with iron-based catalysts showing the highest activity. By applying rational design strategies, numerous research teams have achieved success in improving the ORR activity, electrochemical durability, and membrane electrode assembly (MEA) performance of M–N–C catalysts [11–19]. This chapter will give a synopsis on the current state of knowledge of heat-treated non-PGM catalysts and recent progress in this important area of research.

1.2 Performance Requirements

Traditional non-PGM catalyst performance evaluation in an MEA has been done on a volumetric-activity basis, with the U.S. Department of Energy (U.S. DOE) 2020 target set at 300 A cm^{-3} at a cell voltage of 0.8 V (*iR*-corrected) [20]. To be technologically viable in PEFCs for automotive applications, the performance capabilities of non-PGM catalysts must ultimately meet targets that have also been established for platinum catalysts. For MEAs, these are generally specified on an areal basis and include achieving a current density of 0.3 A cm^{-2} at 0.8 V and a power density of 1.0 W cm^{-2} at rated power. The durability must also be sufficient enough to compete with the capabilities of internal combustion engines. The DOE 2020 target requires that less than 10 % of performance loss (voltage at rated power) after 5000 h of cycling is achieved. While the cycling conditions used are often assumed to be equivalent to 150,000 miles of driving, the ultimate stability testing must also be done under practical conditions (i.e., ambient environments, dynamic loads, and start-up/shutdown) in order to be technologically viable.

In spite of dramatic progress achieved over the past two decades, to the point that non-PGM catalysts have advanced past being considered basic research, [21] the above targets are still very ambitious for non-PGM catalysts. While rotating disc electrode (RDE) and rotating ring disc electrode (RRDE) experiments are very useful for catalyst screening and electrochemical kinetic investigations, MEA integration and performance evaluation in fuel cells have become a priority. Performance improvement investigations need to continue, along with studies to understand the catalyst properties and phenomena that govern performance and stability of electrocatalysts. Only through the application of this knowledge will non-PGM catalysts be capable of achieving established technical targets. If successful, such catalysts will play a key role in reaching the $40 per kW cost targets in place for the automotive-scale PEFC systems [20].

2 Synthesis Path

Jahnke et al. [22] pioneered the use of transition metal macrocycle compounds that contain M–N_4 structures as ORR catalysts. Their research inspired efforts to develop active oxygen reduction catalysts by heat-treating macrocyclic precursors. It was later shown that new synthesis routes for heat-treated transition metal catalysts were successful using less complex ligands, such as sulfates, chlorides, and nitrates. Since that time, several research groups have focused on novel catalyst synthesis and performance improvement [3, 13, 14, 18, 19, 23–36]. Meanwhile, at Los Alamos National Laboratory, Zelenay et al. have been able to increase the activity of Fe–N–C compounds using two heat treatment steps and with proper selection of nitrogen–carbon precursors (e.g., polyaniline and cyanamide) [15, 37]. It is also worth noting that the nature of the non-precious active sites in such heat-treated catalysts is still under debate. This derives from the fact that the function of the transition metal during the catalyst synthesis remains unresolved. Regardless, the catalytic activity was found strongly dependent on the synthesis chemistry, including the structure of the nitrogen precursor transition metals heat treatment temperatures, and inclusion of support materials (i.e., carbon black). On the basis of recent breakthroughs in this field, we will provide a brief outline of the synthesis pathways for such heat-treated M–N–C catalysts. This will be followed by a discussion of the current ORR activity as well as fuel cell performance.

2.1 Precursors

The heat treatment of virtually any mixture of nitrogen, metal, and carbon species can yield a material that displays some ORR activity. To achieve well-performing catalysts, the selection of precursors, supports, and synthesis conditions is much more important. These factors play a major role toward obtaining materials with the high activity and long-term durability required for practical catalysts [38, 39].

2.1.1 Nitrogen–Carbon Precursors

Heat-treated transition metal–nitrogen–carbon catalysts are currently derived from various nitrogen precursors which can be divided into three categories: (i) C≡N-based; (ii) C–N-based; and (iii) aromatic-compound-based precursors. According to the available experimental data, the C≡N and aromatic nitrogen precursors appear to be advantageous over the C–N-based ones in terms of resulting catalyst activity and durability. For example, catalysts derived from heteroatomic polymers show higher activity than catalysts obtained from simple amines, such as ethylenediamine [40]. Two types of polymer-based catalysts were systematically compared using either polyaniline (PANI) or polypyrrole (PPy) as nitrogen

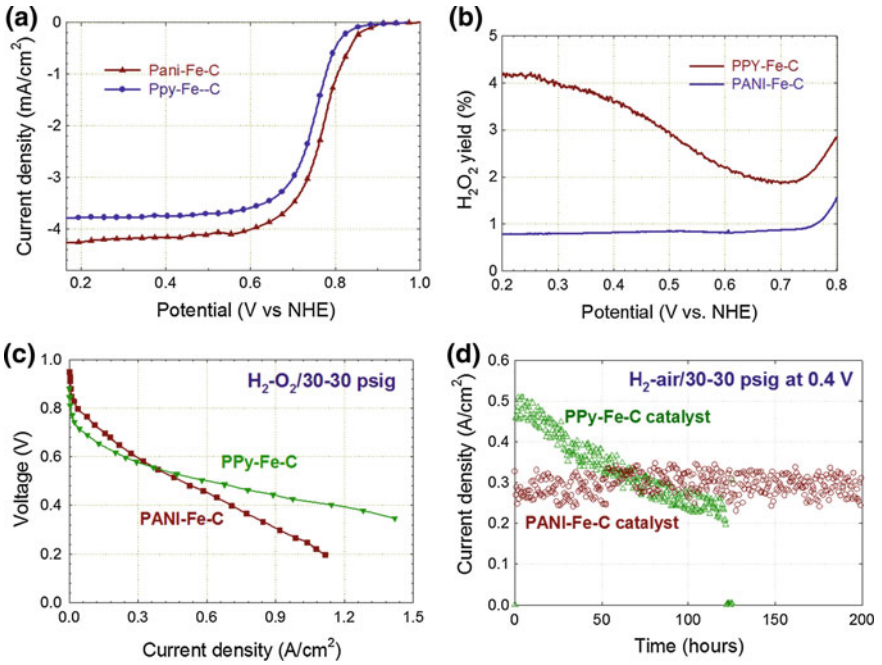

Fig. 1 **a** RDE and **b** RRDE tests for PANI- and PPy-based catalysts. Fuel cell performance of PANI- and PPy-derived catalysts: **c** polarization plots, **d** life tests. Cell temperature 80 °C; anode—0.25 mg cm^{-2} Pt on a woven-web GDL (E-TEK), 30 psig H_2; cathode—catalyst loading 4 mg cm^{-2}; membrane—Nafion® 1135. Reproduced with permission from Ref. [41], copyright (2009) The Electrochemical Society

precursors for catalyst synthesis. As shown in Fig. 1, [41] electrochemical data obtained using RDE shows a lower onset potential (higher overpotential) for oxygen reduction with the PPy–Fe–C (∼0.85 V vs. RHE) than with PANI–Fe–C (∼0.91 V vs. RHE). RRDE results further indicate better selectivity of the PANI-derived catalyst for the four-electron oxygen reduction. The H_2O_2 yield at 0.4 V remains below 1 % for the best performing PANI-derived catalysts.

In good agreement with electrochemical experiments, fuel cell polarization data shown in Fig. 1c confirms higher performance of the PANI–Fe–C catalyst at high cell voltages (>0.55 V). On the other hand, more porous structures of the PPy-derived catalyst benefits performance at lower voltages, where oxygen mass transfer becomes the limited step. Long-term fuel cell performance of both catalysts at a constant voltage of 0.4 V is depicted in Fig. 1d. While PPy–Fe–C shows significantly better activity early in the life test, its performance drops below that of PANI–Fe–C in less than 100 h. On the other hand, PANI–Fe–C exhibits very good stability during the 200-h life test. The difference in the two catalysts' durability may be caused by differences in the nature of the active ORR sites, water tolerance, and/or other factors. There are some indications that precursors with an aromatic

structure may stabilize interactions between the metal and nitrogen species that become embedded into the graphitic structure of the catalyst during heat treatment. This can lead to improved stability of the active reaction sites. This is one possible reason for the much better stability of PANI-derived catalysts.

During the high-temperature catalyst synthesis, one morphological property worth mentioning is that the catalyst structures are dominated by in situ formed graphitized carbon nanostructures, derived from the carbon/nitrogen precursors The appearance of these nanostructures can be correlated to the oxygen reduction activity, providing critical clues in the identification of active sites. Figure 2 shows different carbon nanostructures that result from using various nitrogen/carbon and transition metal precursors during synthesis [42]. Noteworthy, no graphitized carbon structure was formed when polyaniline was heat-treated in the absence of transition metals. This indicates the crucial role of the transition metal in the formation of highly graphitized carbon during heat treatment. The use of ethylenediamine and Co yields an abundance of onion-like carbon nanostructures formed during heat treatment (Fig. 2, top). When cyanamide is used with Fe, bamboo-like carbon nanotubes tend to appear (Fig. 2, mid part). Among the other extensively investigated precursors, polyaniline-derived catalysts are the only ones to demonstrate substantial graphene content following the heat treatment (Fig. 2, bottom). This shows that the aromatic structure of PANI may be a factor in forming graphene, possibly arising due to their structural similarities.

2.1.2 Transition Metal Precursors

Metal-free nitrogen-doped carbon materials exhibit some ORR activity in alkaline media. In the more challenging acidic media, they suffer from inactivity and poor durability. The addition of transition metal(s) is necessary for achieving good catalytic activity and improved durability [43, 44]. Some studies have shown the important effect of the type of transition metal ions used during synthesis on the oxygen reduction activity. Among other approaches, this effect was demonstrated with polyacrylonitrile-derived catalysts and studied in both acidic and alkaline solutions [45]. The nature of the metallic center in the precursors played a governing role on the resultant ORR catalysis. It has become well established that the most active catalysts in acidic electrolyte are formed using either iron or cobalt. Iron-derived catalysts especially have more positive onset potentials than cobalt-derived catalysts, indicating higher intrinsic activity. The iron-containing catalysts also exhibit the highest four-electron selectivity among several other transition metals [45]. In alkaline media, iron- and cobalt-based electrocatalysts often show similar activity [45].

In a recent report, [46] Liao and coworkers systematically studied the effects of the addition of transition metals (Mn, Fe, Co, Ni, Cu) on the structure and performance of doped carbon catalysts derived from PANI and melamine. The results show that the doping of various transition metals significantly affects the structures and performance of the catalysts. Doping with Fe or Mn led to a catalyst with a

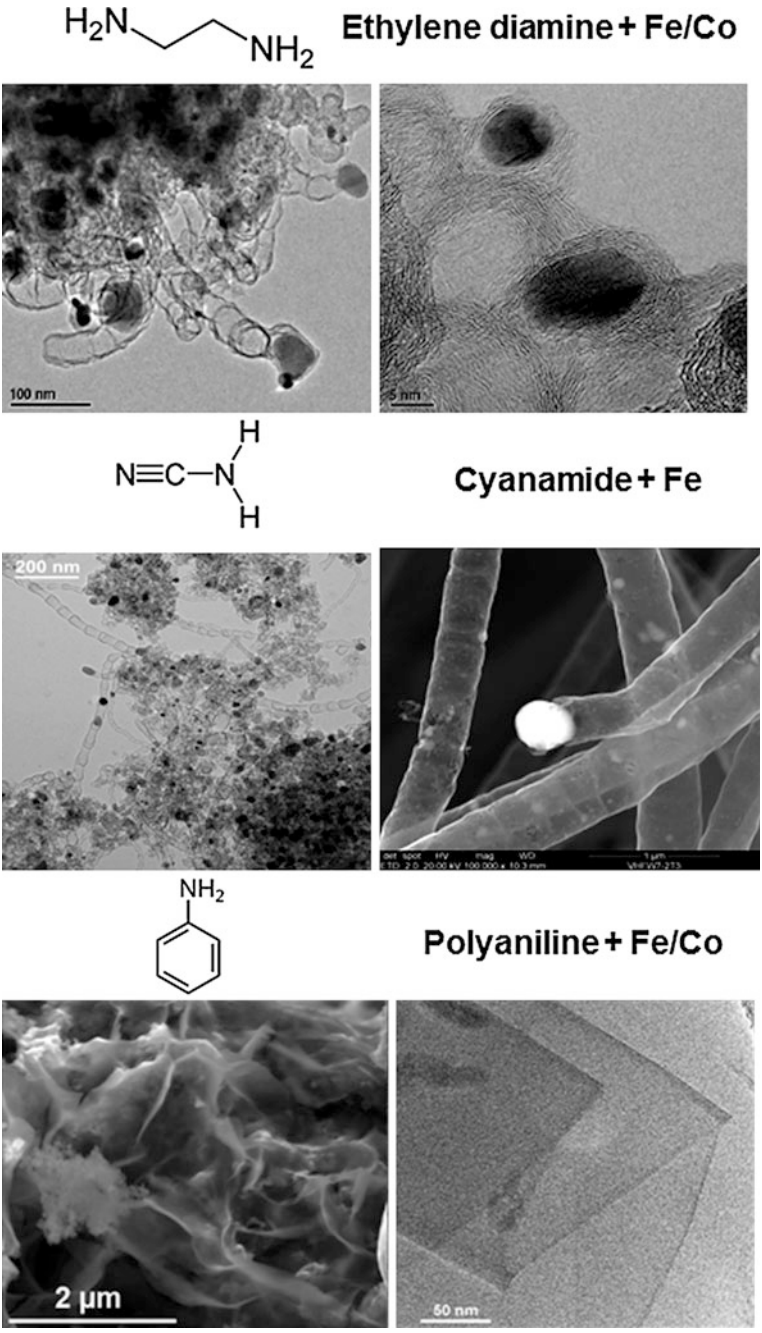

Fig. 2 The various carbon nanostructures observed from the catalysts derived from different nitrogen precursors and transition metal species. Reprinted with permission from Ref. [42], copyright (2012) American Chemical Society

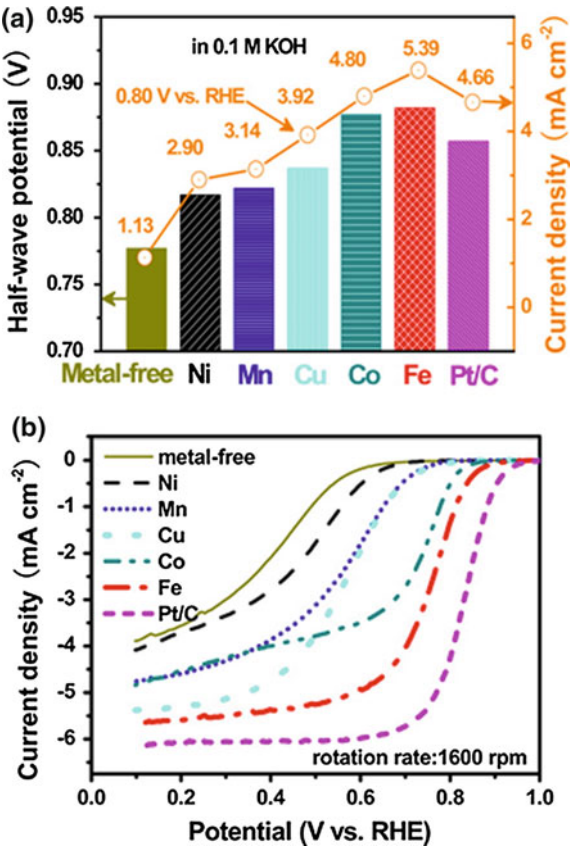

Fig. 3 ORR polarization for catalysts derived from different transition metal precursors in **a** 0.1 M KOH and **b** 0.1 M $HClO_4$ at 298 K. Reprinted with permission from Ref. [46]. Copyright (2014) American Chemical Society

graphene-like structure, whereby doping with Co, Ni, or Cu yielded a disordered or nanosheet structures. As shown in Fig. 3, the doping of transition metals can enhance the performance of the catalysts. The ORR activity of thus doped catalysts in alkaline solution (another order is often observed in acidic electrolytes) decreases in the following order: Fe > Co > Cu > Mn > Ni. It is suggested that this trend is the result of the impact the transition metal has on three properties: (i) the N content of the catalyst, (ii) the amount and type of residual metal species, and (iii) the resulting catalyst surface area and pore structure.

Transition metals can be used for tuning both the morphology of nanostructured carbon and incorporation of nitrogen dopants [10, 37, 38, 42]. As shown in Fig. 4, the carbon nanotube size and doped nitrogen functionalities can be well controlled using different transition metals, such as Ni, Co, and Fe. For example, compared to other metals, Ni-catalyzed carbon nanotubes have the highest pyridinic nitrogen content. On the other hand, Fe is able to yield largest size of carbon nanotubes with relatively high graphitic nitrogen doping. Given the commonly accepted hypothesis that ORR active sites are embedded into the graphitized carbon structures, the

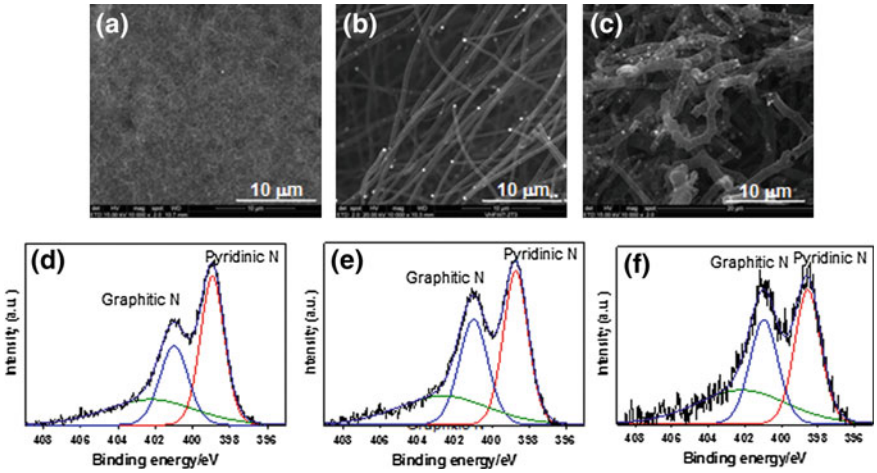

Fig. 4 Nitrogen-doped carbon micro- and nanotubes with the diameter and nitrogen functionalities controlled by the transition metal used in the synthesis: **(a, d)** Ni; **(b, e)** Co, and **(c, f)** Fe. *Top* scanning electron microscopy images; *bottom* corresponding N1s X-ray photoelectron spectroscopy data. Reproduced from Ref. [47] with permission from the Royal Society of Chemistry

highly graphitic nanotubes can offer a potentially attractive host for ORR active sites in these catalysts. By strategically controlling the morphology and N-dopant types/concentrations, improvements to the catalyst performance, durability, and even mass transfer properties are possible.

It was also determined that, in some special cases, the Fe content used for non-PGM catalyst synthesis can play an important role in morphology optimization and activity enhancement [48]. For example, following synthesis involving a nominal iron loading of 30 wt%, the final catalyst had only 2 wt% Fe remaining after acid leach and a second heat treatment. The BET surface area was 845 $m^2\ g^{-1}$, a high value for a non-PGM catalyst supported on Ketjenblack® (KJ) carbon. On the other hand, when using a nominal metal loading of 30 wt% to prepare polyaniline–cobalt–carbon (PANI–Co–C) catalysts, the Co content in the resulting catalyst was 8 wt% and a significantly lower BET surface area was achieved. In good agreement with BET results, the morphology of the catalysts as determined by scanning electron microscopy (SEM) Fig. 4 shows more porosity when higher nominal iron loadings were used for synthesis (Fig. 5) [48]. The highest nominal Fe loading used during synthesis leads to the lowest bulk Fe content in the final catalyst and to the highest BET surface area. This indicates that the in situ formed FeS (with sulfur originating from the ammonium persulfate used as oxidant to polymerize polyaniline) acts as an effective sacrificial pore-forming "template" that is removed during the acid leaching step. It is possible that a higher portion of FeS particles formed with lower Fe loadings of 3 and 10 wt% is fully encapsulated within carbon agglomerates, protecting them during the acid leach step.

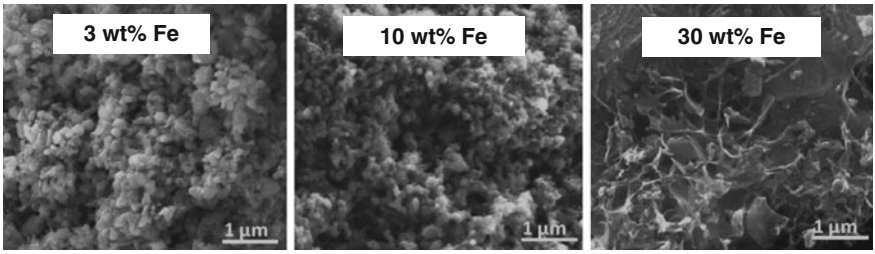

Fig. 5 SEM images of PANI–Fe–C catalysts as a function of Fe loading used during the synthesis. Adapted from Ref. [48]. Reproduced by permission of the American Chemical Society

2.1.3 Effect of Carbon Support

Thanks to their high electronic conductivity, good corrosion resistance, high specific surface area, and falling price, carbon nanotubes have been considered as a replacement for traditional carbon-black supports in fuel cell electrocatalysts. A number of earlier studies have shown that Pt loaded on multi- and single-walled carbon nanotubes exhibits high activity for methanol electro-oxidation and oxygen reduction. Four types of carbon were systematically studied at Los Alamos as supports in non-PGM catalyst synthesis: Vulcan® XC-72, Ketjenblack® 300 J, Black Pearls® 2000, and multi-walled carbon nanotube (MWNTs). Fuel cell polarization plots and life test data for polyaniline–iron (PANI–Fe) catalysts obtained using different carbon supports during synthesis are shown in Fig. 6 [49]. Almost identical polarization plots were observed above 0.35 V, above which MWNT-supported catalysts were found to assure the highest current density, likely thanks to the more open structure of the nanotube-based electrode. MWNTs also benefit the catalyst stability, with virtually no performance degradation after more than 500 h of operation at a cell voltage of 0.40 V. This represents an improvement over the Ketjenblack-supported catalyst that exhibits performance loss already after 200 h of operation.

In general, carbon nanotube (CNT) supports promise improved fuel cell performance over that of traditional carbon blacks. In addition to the excellent electron conductivity, CNTs possess dominant mesoporosity (>2 nm), thus offering better gas permeability and catalytic-site accessibility. Also, water removal within the electrode is facilitated by the hydrophobic nature of the CNT surface, which is of important advantage, especially in the case of non-PGM cathode layers that reach 100 µm in thickness. Higher durability of the MWNT-supported PANI–Fe catalyst may also be related to the higher degree of graphitization of MWNTs, leading to enhanced corrosion resistance and improved stability of the ORR active site(s) [50, 51].

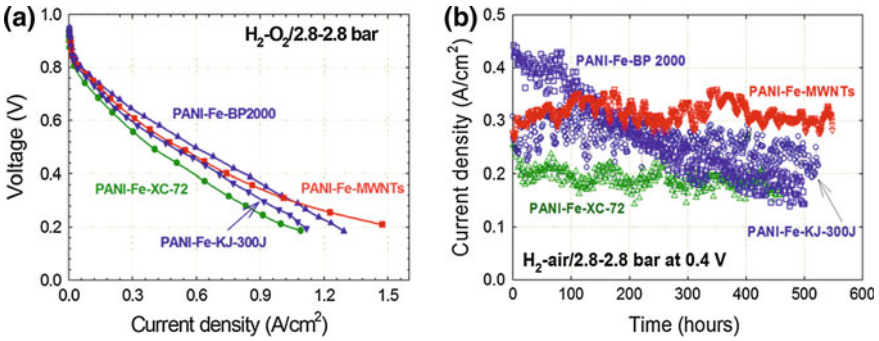

Fig. 6 Fuel cell performance of PANI–Fe catalyst obtained using MWNTs and Ketjenblack as supports: **a** initial polarization plots, **b** life tests. Cell temperature 80 °C; anode—0.25 mg cm^{-2} Pt on a woven-web GDL (E-TEK), 30 psig H_2; cathode—catalyst loading 4.0 mg cm^{-2}; membrane—Nafion® 1135. Adapted from Ref. [49]. Reproduced by permission of The Royal Society of Chemistry

2.2 *Effect of Heating Temperature*

The activity of ORR sites formed in the heat treatment step strongly depends on the temperature used. In research shown in Fig. 7, [15] the ORR activity of the PANI–Fe–C catalyst was studied as a function of temperature ranging from 400 to 1000 °C. The poor activity at 400 °C is very similar to the behavior shown for regular carbons, indicating that no new active sites are formed at low heat treatment temperatures. At temperatures above 600 °C, a significant shift of the ORR onset potential in the positive direction takes place. 900 °C was found to be the optimal temperature in terms of the most positive onset and half-wave potentials.

Elemental analysis of the catalysts heat-treated at different temperatures was determined using X-ray photoelectron spectroscopy (XPS) [38]. It was found that the final Fe content of the catalysts likely increases with the heat treatment

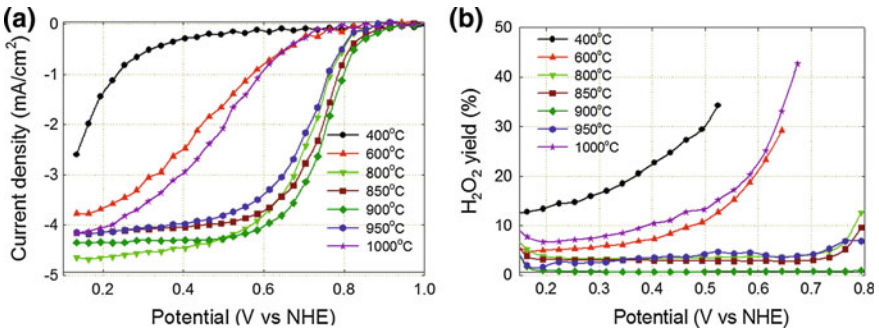

Fig. 7 Effect of heating temperatures on the **a** oxygen reduction activity and **b** four-electron selectivity. Adopted from Ref. [15]. Reproduced by permission of the AAAS

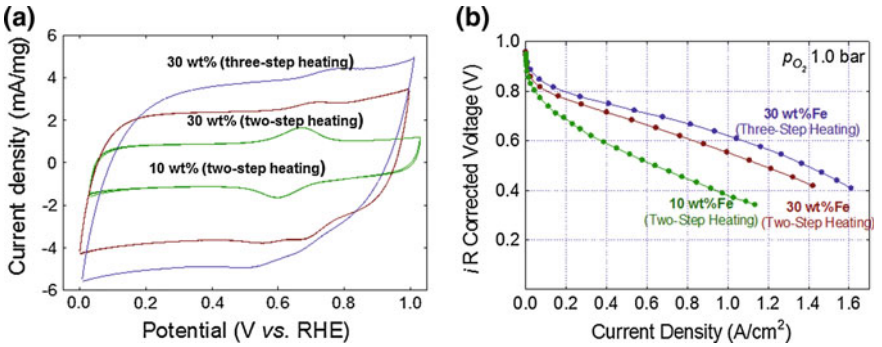

Fig. 8 **a** Cyclic voltammetry and **b** fuel cell performance for various PANI–Fe–C non-PGM catalyst. Cyclic voltammetry: 20 mV s^{-1} in 0.5 M H_2SO_4 solution. Fuel cell tests: Anode: 0.5 mg cm^{-2} Pt (E-TEK) 1.0 bar (partial pressure), H_2, 200 sccm; cathode: ~4.0 mg cm^{-2} 1.0 bar (partial pressure), O_2, 200 sccm; Membrane: Nafion® 211; Cell: 80 °C; 100 % RH

temperature. This is probably due to the enhanced formation of graphitized carbon shells that tend to form around and protect Fe-rich phases at high temperatures. High-resolution transmission electronic microscopy (HRTEM) imaging has repeatedly provided an evidence for that interpretation [48]. An increase in the heat treatment temperature also leads to an increase in the carbon formed in PANI carbonization. Interestingly, the nitrogen content decreases with an increase in the heating temperature from 600 to 900 °C, which is not accompanied by a drop in ORR activity. This suggests that catalyst activity is not entirely dependent on the total amount of doped nitrogen, as claimed by some researchers, [38] but is strongly related to the doping position and local atomic environment.

Beside the heat treatment temperature, the number of heating steps has been found to affect the ORR activity of non-PGM catalysts. Recently, a novel three-step heating strategy to prepare high-surface-area Fe catalysts was developed at Los Alamos [48]. The new cathode catalysts were found to have much increased electrochemically accessible surface area relative to the traditional two-step synthesis (Fig. 8a). A current density of 190 mA cm^{-2} at a voltage of 0.80 V (*iR*-free) was achieved in fuel cell testing using this strategy (Fig. 8b).

3 Performance Evaluation and Catalyst Characterization Techniques

3.1 Electrochemical Cell Testing

Electrochemical cell testing is a simple and convenient approach to measuring the ORR activity and H_2O_2 yield. Among numerous electrochemical techniques, the most important and widely used are the RDE and RRDE methods.

3.1.1 Electrochemical Cell Set-up

Glass cells equipped with three electrodes are usually used in electrochemical testing. A thorough cleaning of the glassware is essential to eliminate impurities that negatively affect ORR activity of catalysts. A typical cleaning procedure involves soaking the glassware in a mixture of concentrated sulfuric acid and an inorganic oxidizer, such as Nochromix (GODAX Laboratories, Inc.), and then rinsing them with deionized (DI) water (18 MΩ cm). Acid electrolyte (e.g., 0.5 M H_2SO_4, 0.1 M $HClO_4$) or alkaline electrolyte, (e.g., 0.1 M KOH) is chosen depending on the application of interest. In selecting a reference electrode, it is most appropriate to choose a reference electrode that shares the same anion as the electrolyte, such as the mercury–mercurous sulfate electrode (MSE, 0.68 V vs. NHE) when using sulfuric acid electrolyte. All potentials measured versus a reference electrode should be converted into the reversible hydrogen electrode (RHE) scale to facilitate comparison of results from different laboratories. In order to avoid any potential contamination of the non-PGM catalyst with platinum or other precious metals, the use of a graphite rod as a counter electrode is suggested. RDE using a glassy carbon disk and RRDE made up of a glassy carbon disk surrounded by a platinum ring are typically used as working electrodes. The non-PGM catalysts are ultrasonically dispersed in an alcoholic solution containing suspended Nafion® ionomer to form a catalyst "ink" that is applied to the glassy carbon disk surface. At Los Alamos National Laboratory, the catalyst ink is usually prepared by ultrasonically blending for 1 h 10 mg of the non-PGM catalysts and 40 μl of 5 wt% Nafion® suspension in alcohol (Solution Technology, Inc.) in 2.0 mL isopropanol. Homogeneous catalyst deposition onto the glassy carbon electrode is very important for obtaining reliable and reproducible electrochemical data.

3.1.2 RDE/RRDE Measurements

RDE and RRDE measurements are usually performed using a computer-controlled potentiostat and a rotator. RDE is a simple and convenient screening tool for assessing ORR activity of newly developed non-PGM catalysts. One way of evaluating the ORR activity is to measure the half-wave potential ($E_{½}$). This is the potential at which the current density is equal to one-half of the mass-transport limited current density (Fig. 9). A higher $E_{½}$ corresponds to higher ORR activity (for a given catalyst loading). The other way of estimating ORR activity is to measure the current density in the kinetic region, such as at an electrode potential of 0.90 V versus RHE.

Linear sweep voltammetry (LSV) is usually conducted with the electrode immersed in deoxygenated electrolyte prior to carrying out LSV in oxygen-saturated electrolyte. The ORR polarization curve is obtained by subtracting the LSV measured in deoxygenated electrolyte from the LSV measured in oxygen-saturated electrolyte, whereby capacitive currents can be eliminated. As higher LSV

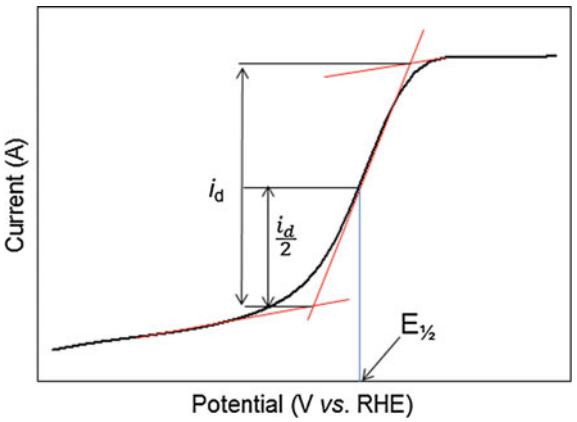

Fig. 9 Half-wave potential ($E_{½}$) determination in RDE testing

scan rates lead to higher $E_{½}$ and higher current densities in the kinetic region, the scan rate is important in reporting ORR performance and needs to be specified. Slow scan rates (5–10 mV s^{-1}) are recommended for recording ORR polarization plots with non-PGM catalysts. At Los Alamos National Laboratory, steady-state measurements have been adopted to obtain ORR polarization plots. These are recorded in oxygen-saturated electrolytes, starting at the open cell potential (OCP) and decreasing it stepwise, typically by 20 or 30 mV, with a hold time of 30–60 s, down to 0.0 V versus RHE. A 120-s potential hold at the open-circuit potential precedes every ORR polarization experiment.

The kinetic current (i_k) and average number of electrons transferred per oxygen molecule (n) can be obtained through RDE experiments using the Koutecky–Levich equation (Eq. 1):

$$\frac{1}{i} = \frac{1}{i_k} + \frac{1}{i_D} = \frac{1}{i_k} + \left(\frac{1}{0.62nFD^{\frac{2}{3}}v^{-1/6}C_O}\right)\omega^{-1/2} \tag{1}$$

Here, i is the measured current density, i_k is the kinetic current density, i_D is the diffusion limited current density, n is the number of electrons transferred per oxygen molecule, F is the Faraday constant (96485 C mol^{-1}), D is the diffusion coefficient of the molecular O_2, C_O is the concentration of molecular O_2 in the electrolyte, v is the kinematic viscosity of electrolyte, and ω is the angular rotation rate (rad s^{-1}). Plotting $\frac{1}{i}$ versus. $\omega^{-1/2}$ yields n from the slope and i_k from the intercept on the $\frac{1}{i}$ axis. The i_k obtained from the Koutecky–Levich plot can also be utilized to obtain the Tafel plot, logi_k versus E, to determine the Tafel slope and exchange current density (i_0).

The theoretical limiting current density in RDE experiments can be calculated using Levich Eq. 2:

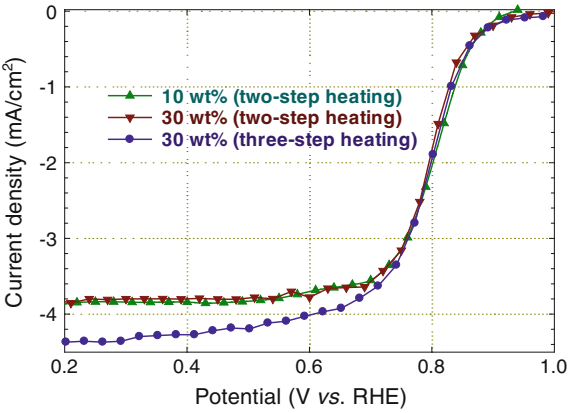

Fig. 10 RDE performance with three different Fe–PANI–C catalysts

$$i_L = 0.62nFAD^{2/3}\omega^{1/2}\nu^{-1/6}\mathrm{C_O} \tag{2}$$

Here, i_L is the limiting current and A is the electrode area.

Using RRDE, H_2O_2 yield can be measured based on Eq. 3 by setting the ring potential for H_2O_2 oxidation to ca. 1.4 V versus RHE:

$$\mathrm{H_2O_2}(\%) = 200 \times \frac{i_R/N}{(i_R/N) + i_D} \tag{3}$$

Here, i_D and i_R are the disk and ring current densities, respectively, and N is the ring collection efficiency $\left(N = \left|\frac{i_R}{i_D}\right|\left(\frac{n_D}{n_R}\right)\right)$. The peroxide yield can be directly correlated to the average number of electrons transferred per O_2 molecule (n) through the following:

$$n = 4 - (\%\mathrm{H_2O_2})/50\,\% \tag{4}$$

One should keep in mind though that RDE ORR performance of a catalyst does not always reflect its fuel cell performance. This consideration holds true for non-PGM catalysts in particular. For example, test data shown for three PANI–Fe–C catalysts in Fig. 8b above attest to a major performance differences in the fuel cell, which is not at all reflected in the RDE testing (Fig. 10). Among possible reasons for the observed discrepancy between the RDE and fuel cell performance, water generation may be of particular importance. While obviously having no impact on RDE performance of catalysts, it can significantly influence the fuel cell performance by affecting the oxygen access to the active sites in the fuel cell cathode.

3.2 Fuel Cell Testing

Testing of non-PGM catalysts in the fuel cell cathode is of utmost significance for the evaluation of their activity and durability under PEFC operating conditions. MEA fabrication is thus an important element of a non-PGM catalyst evaluation. Typically, a catalyst "ink" is first prepared by ultrasonically mixing the catalyst powder with a Nafion® suspension for 3–4 h. One commonly used ink composition at Los Alamos National Laboratory to obtain a catalyst layer containing 35 wt% of Nafion® involves mixing of a non-PGM catalyst, water, isopropanol, and a 5 wt% of Nafion® suspension in a weight ratio of 1:12:12:11, respectively. The ink is then applied to the membrane or gas diffusion layer by successive brush painting (or spraying) until a target cathode catalyst loading is reached on a vacuum hot plate maintained at 80 °C. Commercial Pt-catalyzed carbon paper (0.2 mg_{Pt} cm^{-2}) is normally used at the anode. The gasket thickness is chosen to be *ca*. 80 % of the uncompressed (gas diffusion layer + catalyst layer) thickness. The cathode and anode are hot-pressed at 80–120 °C for 5 min onto a piece of a Nafion® membrane. In some cases, two membranes are used. This approach minimizes the risk of a possible cross-contamination of the cathode with Pt from the anode during MEA preparation and also facilitates postmortem characterization of the individual fuel cell electrodes. Figure 11 shows the comparison of fuel cell performance of single- and two-membrane MEAs with non-PGM catalysts. As shown in Fig. 11a, the double membrane MEA exhibits a higher high-frequency resistance (HFR) and lower performance at the mass-transport limited region. However, comparison of the *iR*-corrected polarization plots reveals identical performance of both MEAs (Fig. 11b).

Recommended fuel cell test conditions include the use of pure hydrogen and air/oxygen, humidified at 80 °C to assure 100 % relative humidity at an anode stoichiometry of 2 and cathode stoichiometry of 9.5. Both electrodes should be maintained at a backpressure that results in a 1.0 bar partial pressure of the gases. Testing is typically carried out a cell temperature of 80 °C.

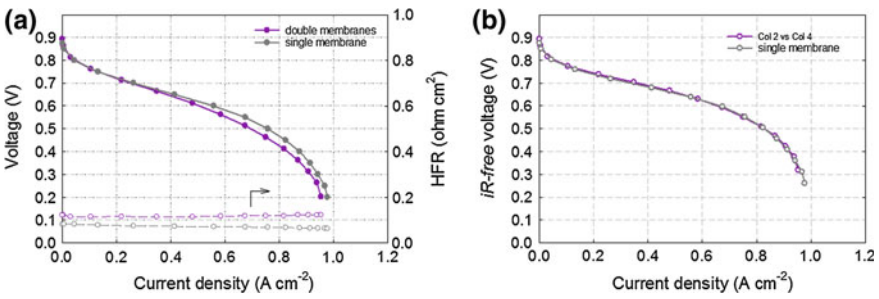

Fig. 11 Fuel cell performance of MEAs single and double MEAs: **a** before and **b** after *iR*-correction

3.3 Physicochemical Characterization Techniques

Heat-treated non-PGM catalysts have a complex structure, usually consisting of carbon (*ca.* 90 at.%), nitrogen (*ca.,* 5 at.%), metal (most commonly Fe or Co, *ca.* 2 at.%), and other elements (e.g., O, *ca.* 3 at.%). A systematic study of catalysts prepared by various synthesis paths is of importance for gaining insight into the structure and for improving ORR performance and stability of the catalysts. Since nitrogen, iron, and carbon are the main elements in non-PGM ORR catalysts, we will concentrate below on techniques that particularly useful in the analysis of these elements.

XPS is the most common technique to determine elemental composition of non-PGM catalysts. In particular, XPS is an excellent tool to ascertain the type and relative amount of nitrogen functionalities doped into carbon through deconvolution of high-resolution N1s spectra (Detailed analysis of C1s spectra is difficult due to the lack of distinct spectral features.). The valence state of metals in catalysts can be established by the deconvolution of metal spectra. XPS is often referred to as a surface-sensitive technique but in reality the information obtained is not limited to the catalyst surface. Since ORR is strictly a surface reaction, it is important to know the sampling depth of XPS for non-PGM catalysts to conclude how relevant XPS signatures are to the catalyst surface. Universal curves of electron inelastic mean free path curve for either Mg Kα X-ray (1253.6 eV) or Al Kα X-ray (1486.6 eV) sources, typically used in XPS, reveal the sampling (escape) depth for carbon, i.e., the depth from which 95 % of all photoelectrons are absorbed by the time they reach the surface is *ca.* 6 nm. In the case of carbon, the distance between graphene planes is *ca.* 0.34 nm. Thus, the XPS information from carbon-based non-PGM catalysts originates from *ca.* 20 atomic layers of carbon. By lowering the angle between the X-ray source and the sample, more surface-specific information can be obtained.

X-ray absorption spectroscopy (XAS) is another widely used tool for analyzing the structure of non-PGM catalysts. Depending on the X-ray energy range, carbon (280–300 eV), nitrogen (390–420 eV), and iron (7100–7200 eV) spectra can be obtained. An X-ray absorption spectrum is generally divided into four sections: (i) pre-edge, $E < E_0$ (binding energy); (ii) X-ray absorption near-edge structure (XANES), $E = E_0$ up to E_0 + *ca.* 10 eV); (iii) near-edge X-ray absorption fine structure (NEXAFS), $E = E_0$ + *ca.* 10 eV to E_0 + *ca.* 50 eV; and (iv) extended X-ray absorption fine structure (EXAFS), $E = E_0$ + *ca.* 50 eV to E_0 + *ca.* 1000 eV. In carbon NEXAFS, the relative amount of unsaturated carbon bonds (sp or sp^2) and saturated carbon bonds (sp^3) can be assessed by comparing 1 s $\rightarrow \pi^*$ carbon spectra (284–288 eV) and 1 s $\rightarrow \sigma^*$ carbon spectra (*ca.* 290 eV). The presence of a π^* resonance in the low-energy range of the carbon spectra is characteristic of unsaturated (sp or sp^2) carbon bonds. However, for diamond which is purely sp^3-bonded, no π^* resonance is observed, only 1 s $\rightarrow \sigma^*$ transition at *ca.* 290 eV. Nitrogen analysis for non-PGM catalysts with NEXAFS is difficult due to the low doping level of nitrogen in the catalysts. The oxidation state of iron can be

measured by XANES, while the coordination number of the iron center and type of direct neighboring atoms can be identified by EXAFS.

Raman spectroscopy is also useful tool for structural analysis of non-PGM catalysts. However, the complexity of the carbon phase in such catalysts makes interpretation of Raman spectra very difficult. Raman spectra are affected by the ratio of sp^2/sp^3 bonds, crystallite size, bond-angle disorder, bond-length disorder, heteroatoms, etc. [52]. Generally, the spectra around 1580 cm^{-1} (G band) and 1350 cm^{-1} (D band) are known to correspond to the planar motion of sp^2-hybridized carbon atoms in an ideal graphene layer and carbon atoms close to the edge of a graphene sheet, respectively [53]. The D band is inversely proportional to the crystallite size. The ratio of I(D)/I(G) (where I denotes the band intensity) is often used to measure the degree of disorder in the graphene layer. The relative concentration of amorphous carbon could be assessed from G and D bands in the Raman spectra.

The morphology of non-PGM catalysts can be studied by SEM and TEM. Combining these techniques with energy-dispersive X-ray spectroscopy (EDS) makes elemental mapping possible. The specific surface area, total pore volume, and pore-size distribution are important parameters that play a key role in the ORR performance of non-PGM catalysts. The Brunauer–Emmett–Teller (BET) method is widely used to determine the surface area of solid materials. Before measurements the samples are degassed under a nitrogen flow at *ca.* 250 °C for approximately 5 h to ensure the removal of adsorbed water. The W_m, the weight of adsorbate (mostly N_2) constituting a monolayer of surface coverage, is obtained from the BET isotherm using the following equation:

$$\frac{1}{W(P_0/P-1)} = \frac{1}{W_m C} + \frac{C-1}{W_m C}\left(\frac{P}{P_0}\right) \tag{5}$$

Here, W is the weight of gas adsorbed at a relative pressure P/P_0. The total surface area S_t of the sample is calculated from W_m:

$$S_t = \frac{W_m N A_{\mathrm{cs}}}{M} \tag{6}$$

Here, N is the Avogadro's constant (6.022×10^{23}), M is the molar mass of the adsorbate (14 for N_2), and A_{cs} is the cross-sectional area of the adsorbate (16.2 $Å^2$ for nitrogen). The total pore volume is derived from the amount of vapor adsorbed (V_{ads}) at a relative pressure close to unity by assuming that the pores are then filed with liquid adsorbate (V_{liq}) as follows:

$$V_{\mathrm{liq}} = \frac{P_a V_{\mathrm{ads}} V_m}{RT} \tag{7}$$

Here, P_a and T are ambient pressure and absolute temperature, respectively, and V_m is the molar volume of the liquid adsorbate (34.7 cm^3 mol^{-1} for nitrogen). The

pore-size distribution is calculated based on the pore-size dependence of adsorbate condensation (evaporation) a specific P/P_0, using several available models in the calculation. The pores are classified as macro-, meso-, and microporos for the diameter greater than 500 Å, between 20 and 500 Å, and smaller than 20 Å, respectively.

4 Catalyst Structure

4.1 The Active Site Debate

In the synthesis of M–N–C catalysts, significant structural and chemical changes occur during the heat treatment. For this reason, a complex mixture of various species results, including both graphitic and amorphous carbon structures, along with the presence of doped nitrogen species, as well as metal oxides, sulfides, and carbides [54]. Because of the highly heterogeneous structure of these catalysts, elucidating the exact identity of the active site structure(s) has been a difficult endeavor and subject of contention in the scientific community. This has been further complicated by the fact that not only the atomic identity of the active site can govern M–N–C activity, but the surrounding environment can play a role owing to induced electronic and geometric effects [55–57]. Establishing this fundamental understanding regarding the active site identity (identities) is, however, highly desirable as it will provide a missing piece of information that can be used to guide improved catalyst designs and mechanistic studies.

An intense debate remains on whether or not metal species are an integral component of the ORR active site, [8] with iron-based catalysts being the most extensively investigated. Some researchers assert that metal species are actually not present in the active site structures, although transition metals, Fe in particular, play a crucial role in facilitating the formation of highly active nitrogen–carbon moieties [58, 59]. This can be used to explain the dramatic performance enhancement achieved upon the addition of even small amounts of transition metal precursors [58, 60]. This activity remains following an acid leach performed to remove metal-based species, as confirmed by surface-specific characterization, such as XPS. Other research teams strongly believe that the active site involves metal ions, e.g., $Fe^{2+/3+}$, directly coordinated to nitrogen species [57, 61, 62]. Nitrogen coordination is viewed as providing a relatively stable configuration that is not prone to removal during acid leaching or under the electrochemical conditions encountered during ORR activity evaluation. This Fe–N_4/C arrangement also implies a commonality between transition metal macrocycle complexes that have been shown to be ORR active, albeit with limited activity and electrochemical stability [63, 64]. The most common notion for a metal-based active site is that Fe ions are coordinated by four nitrogen species. This for example includes the FeN_4/C (Fig. 12a) or FeN_{2+2}/C (Fig. 12b, c) structures. Of these different species, it is the FeN_4/C

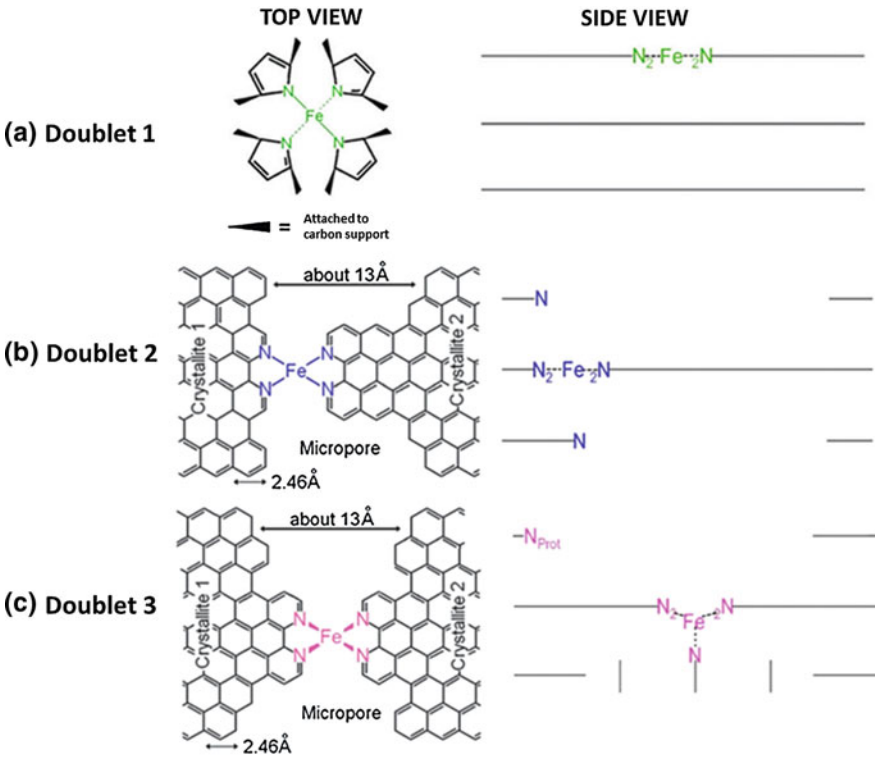

Fig. 12 Schematic representation of the iron–nitrogen coordinated sites observed using Mössbauer spectroscopy for catalysts prepared by heat-treating a mixture of iron acetate and carbon black in ammonia. Depicted are **a** FeN_4/C, **b** FeN_{2+2}/C, and **c** five-nitrogen coordinated N–FeN_{2+2}/C. The majority of ORR activity is attributed to sites **(a)** and **(c)**. Adapted from Ref. [57] with permission of the PCCP Owner Societies

(Fig. 12a) and N–FeN_{2+2}/C structure with a fifth coordinated nitrogen (Fig. 12c) that were found to be responsible for ORR activity in catalysts prepared by heat-treating a mixture of iron acetate and carbon black in ammonia [57]. Particularly, the N–FeN_{2+2}/C structure was unique to catalysts that were subjected to a heat treatment in ammonia. MEA performance variations of ammonia-treated catalysts were also later ascribed to increased reactant accessibility induced by ammonia treatment [12].

The other debate in the non-PGM catalyst community is whether or not there is a second active site species at play. Hydrogen peroxide is commonly produced as an intermediate or ORR by-product. Serov et al. [29] based on an observed loading dependence on RDE activity showed that the ORR occurs by a 2 × 2 electron reduction mechanism on catalysts prepared by heat-treating a mixture of iron chloride, polyethyleneimine, and carbon black. This unveils the rather complicated mechanism of oxygen reduction, as the generated hydrogen peroxide could very

likely undergo chemical decomposition (forming oxygen and hydrogen) or be electrochemically reduced to water. The extent of each of these occurrences is unknown and difficult to differentiate through experimentation. Based on results from in situ XAS experiments, Mukerjee et al. [25] claimed that the first 2-electron reduction of oxygen to hydrogen peroxide occurs on the aforementioned FeN_4/C moieties. These hydrogen peroxide species then migrate to a secondary active site where they are electrochemically reduced, resulting in an overall four-electron process.

The theories and hypotheses proposed are traditionally based on results from an array of surface and structural characterization techniques that are linked to catalyst performance evaluation (discussed in Sect. 3). It is also very likely that the real identity and behavior of the active site structure(s) in non-PGM catalysts is material-dependent and relates to the particular synthesis procedures and conditions selected. It is therefore important to gain a fundamental understanding into each particular system of M–N–C catalysts. Along with overlying trends, established in the field of non-PGM catalysis, this progress is essential toward achieving an established PEFC performance metrics.

4.2 Mass Transport Facilitation

As non-PGM catalysts are only a fraction of the cost of conventionally used precious metals, it is economically possible to use significantly higher loadings in the catalyst layer to achieve performance targets. The non-PGM catalyst layers in fuel cells are as much as 100 μm in thickness. At this length scale, mass transport through both the electrode and catalyst structures becomes an important technological challenge that must be addressed [14, 65]. If the developed catalysts have poor intrinsic mass-transport properties, electrode utilization will be very poor and PEFC performance will suffer accordingly. It has become well established that a high content of meso- and macropores is important for the efficient transport of ORR species [12, 57]. This includes the access of oxygen and proton to the catalytically active sites, along with the removal of the product water. To capitalize on the many recent advances, which have dramatically increased the intrinsic ORR activity of heat-treated M–N–C catalysts, rational meso- and macrostructure design strategies must be applied to facilitate effective mass transport. To accomplish this, a few different catalyst preparation strategies have been employed with varying degrees of success.

Serov et al. [66–68] have incorporated silica templates into the reaction mixture that consists of iron, nitrogen, and carbon precursors. The overall synthesis procedure is depicted in Fig. 13a. After a high-temperature heat treatment, the silica template particles are removed using an etching reagent, such as hydrofluoric acid. What remains are highly porous structures that are inverse replicas of the initial silica templates. By this approach, pore size and property tuning can be made by deliberate selection of the silica templates being employed. This not only allows for

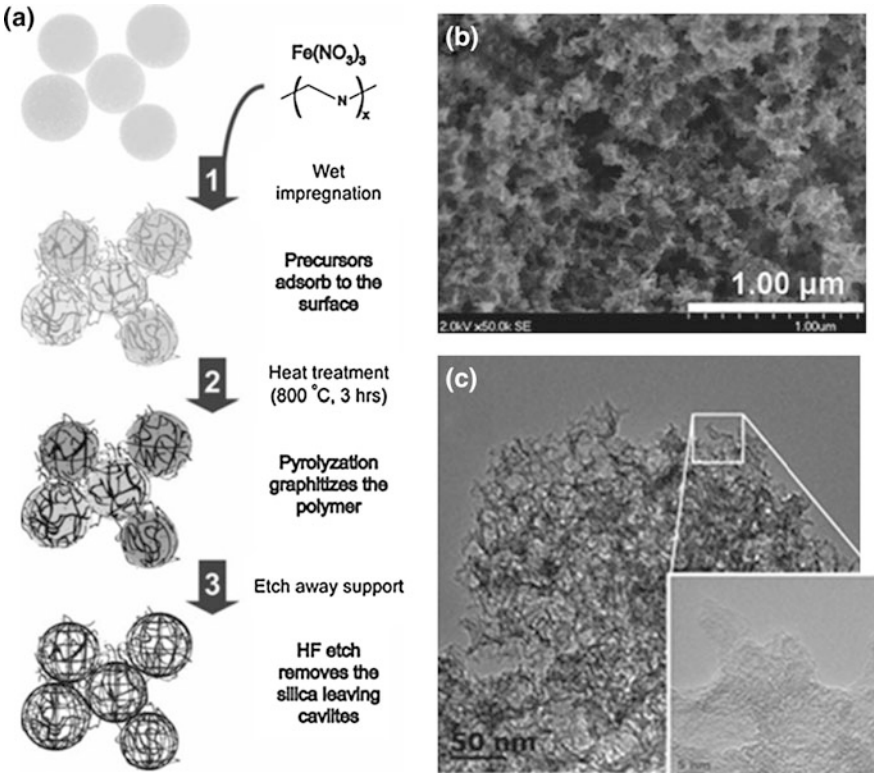

Fig. 13 **a** Schematic representation of the sacrificial support method to prepare catalysts, in which iron, nitrogen, and carbon precursors are mixed with silica templates. After heat treatment, the silica templates are removed by hydrofluoric acid. Reprinted from Ref. [66] Copyright (2012), with permission from Elsevier. **b, c** Transmission and scanning electron microscopy images, respectively, of high-surface-area M–N–C catalysts prepared by the sacrificial support method using 30-nm silica templating particles. Reprinted with permission from Ref. [18], copyright Wiley

practical performance gains realized using this technique, but also provides valuable opportunity to generate fundamental information regarding the effect of pore sizes and structures on catalyst activity and MEA performance. Using 30-nm silica particles mixed with iron nitrate and carbendazim [18] these authors prepared highly mesoporous catalysts using a heat treatment and successive hydrofluoric acid etching (Fig. 13b, c). Upon integration into electrode structures for H_2–O_2 MEA evaluation, areal current densities of 120 and 700 mA cm^{-2} were achieved at cell voltages of 0.8 and 0.6 V, respectively (no *iR*-correction).

Another interesting approach taken to structurally control M–N–C catalysts was first pioneered by Ma et al. [69] and involves metal-organic framework (MOF)-derived catalysts. In this work they heat-treated an in-house prepared cobalt imidazolate MOF to prepare a catalyst that showed promising half-cell electrochemical activity toward oxygen reduction. Proietti et al. [14] advanced on this work, instead

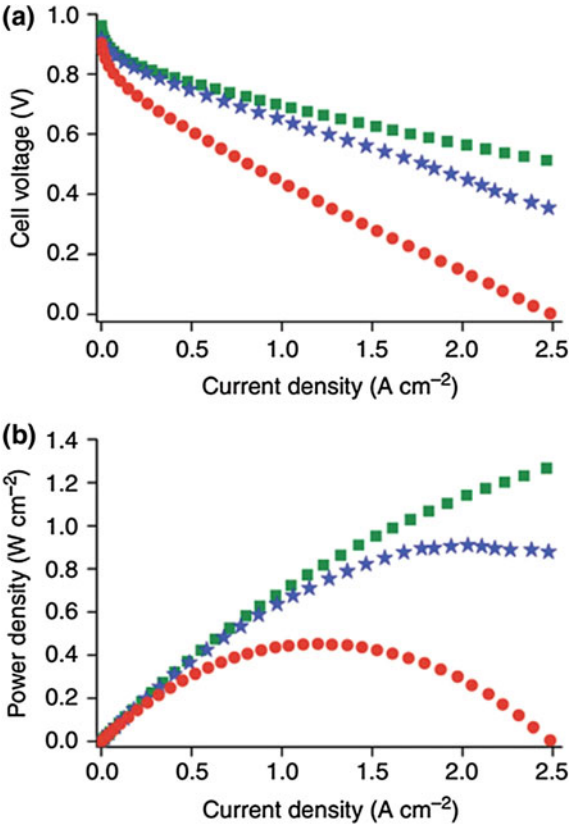

Fig. 14 **a** Polarization curves (H_2–O_2) and **b** corresponding power density curves for (*green squares*) state-of-the-art platinum-based cathode with 0.3 mg_{Pt} cm^{-2} loading, (*blue stars*) best performing zinc imidazolate framework-derived catalyst [14] and (*red dots*) the author's previously reported most active iron-based catalyst. Adapted from Ref. [13]. Reprinted by permission from Macmillan Publishers Ltd: [14] copyright (2011)

using a commercial zinc imidazolate framework mixed with 1,10-phenanthroline and iron acetate. These were chosen as iron and nitrogen precursors owing to the authors' previous investigations [13]. Interestingly, after an initial heat treatment in argon and subsequent heat treatment in ammonia, a highly porous catalyst resulted with a high content of both mesopores and micropores [14]. By combining high activity of the optimized catalyst technology with the excellent mass-transport properties arising from the structure, a current density of 1.25 A cm^{-2} at 0.6 V under H_2–O_2 conditions was achieved, corresponding to a power density of 750 mW cm^{-2} (Fig. 14). This MOF approach is relatively straightforward and feasible; however, only a limited number of MOFs are commercially available. The other alternative is to synthesize the templates in house, where tailoring the structure of the nitrogen ligands in zinc-based MOFs was demonstrated by Zhao et al. [16]. This resulted in different structures of the resulting heat-treated M–N–C catalysts, with the optimal formulation developed by these authors providing a peak power density of 620 mW cm^{-2} at 0.43 V.

Recently, a new method has been developed at Los Alamos National Laboratory to generate highly porous structures using a combined nitrogen precursor approach

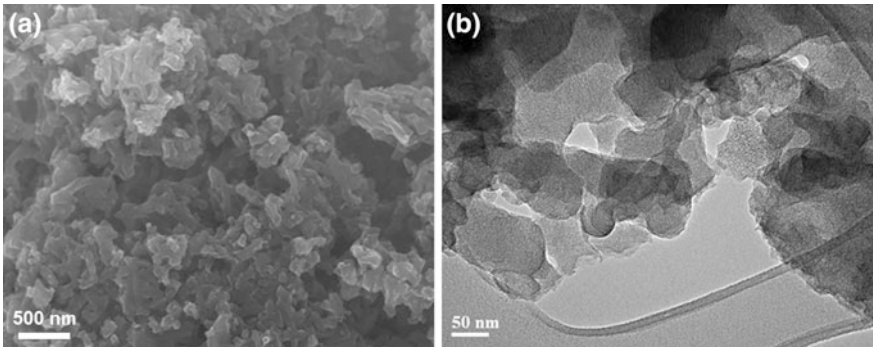

Fig. 15 **a** Scanning and **b** transmission electron microscopy images of highly porous M–N–C derived from the mixed nitrogen precursor approach, using both cyanamide and polyaniline in tandem

[21]. In the method, cyanamide and iron chloride are mixed together, followed by the addition of aniline and subsequent polymerization. Both cyanamide and polyaniline have been previously shown as highly effective precursors [15, 40, 41, 70, 71]. In this work, cyanamide plays an additional role of acting as a pore-forming agent. This technique thereby alleviates the reliance on hazardous etching reagents to remove templates (i.e., hydrofluoric acid) and does not require the inclusion of precursor species that are not involved in active site formation (i.e., zinc). After the addition of carbon black, the precursor mixture is subject to a first heat treatment in argon. The materials are then acid-leached to remove surface inactive species, and a second heat treatment is done in argon. The resulting catalyst is highly porous, including a microporous surface area of more than 1500 $m^2\ g^{-1}$ and a large content of mesopores observed through electron microscopy (Fig. 15). This structural arrangement translates to high performance in an H_2–O_2 and H_2-air tested MEA, including a power density of 870 mW cm^{-2} at 0.4 V and 380 mW cm^{-2} at 0.50 V, respectively.

It is important that the mass-transport properties of heat-treated M–N–C catalysts be taken into consideration when attempting to translate excellent ORR kinetics into practical fuel cell performance. Strategies must continue to be developed that are effective at simultaneously providing electrokinetic improvements, along with excellent active site accessibility throughout the relatively thick non-PGM catalyst layers.

5 Summary

Although the fuel cell performance of heat-treated non-PGM catalysts has been dramatically improved over the past two decades, further improvements are still required to compete with state-of-the-art Pt catalysts. Due to the fact that an

essential heat treatment of a combination of nitrogen precursors metal precursors, and carbon supports produces catalysts with varying degrees of ORR activity, researchers have been led to adopt a variety of precursors and synthetic approaches to advance non-PGM catalyst development. Though indispensable, the heat treatment destroys the initial structure of precursors, producing a highly heterogeneous, complicated structure that makes it very difficult to elucidate and understand the active site(s) of the resulting non-PGM catalysts. For this reason, the development of non-PGM catalysts depends more on a trial-and-error type approach, rather than scientific studies that are rationally guided by fundamental knowledge surrounding the active site structure(s) and their formation. It is therefore becoming increasingly clear that active site understanding is required in order to propel non-PGM catalyst development to new levels of achievement. According to published papers about non-PGM catalysts, the nitrogen precursor selection plays one of the most important roles in governing ORR activity when comparing a variety of different non-PGM catalysts. Therefore, understanding how the structure and properties of the different nitrogen precursors influence the nanostructure, surface properties, and activity of the resultant catalysts after heat treatment is an important starting point.

Another important issue related to this type of non-PGM catalysts is durability. Until now, no non-PGM catalyst has been demonstrated to be durable under practical PEFC operating conditions. From the practical application viewpoint, durability is as important as performance. Therefore, understanding the cause of performance loss of this type of non-PGM catalysts and developing durable alternatives are also an urgent research field. Applying a host of diverse physicochemical analysis tools in conjunction with electrochemical and fuel cell tests is crucial in this endeavor, and has been the focus of a large number of investigations. Considering the complex structure of non-PGM catalysts, thorough investigations must be carried out that provide fundamental insight, exceeding these now "routine" studies. Sophisticated techniques, including a host of both microscopy and spectroscopy experiments are required in tandem, with the ability to investigate catalysts in situ (either in "half-cell" or MEA), potentially providing the key to breakthroughs in terms of elucidating the active site structure(s) of the most active non-PGM catalysts prepared to date.

References

1. U.S. Department of Energy's 2014 Annual Merit Review and Peer Evaluation Meeting Presentation (2014) Fuel cell transportation cost analysis. http://www.hydrogen.energy.gov/pdfs/review14/fc018_james_2014_o.pdf
2. Bing Y, Liu H, Zhang L, Ghosh D, Zhang J (2010) Nanostructured Pt-alloy electrocatalysts for PEM fuel cell oxygen reduction reaction. Chem Soc Rev 39:2184–2202
3. Higgins D, Hoque MA, Seo MH, Wang R, Hassan F, Choi JY, Pritzker M, Yu A, Zhang JJ, Chen Z (2014) Development and simulation of sulfur-doped graphene supported platinum with exemplary stability and activity towards oxygen reduction. Adv Funct Mater 24: 4325–4336

4. Higgins DC, Wang R, Hoque MA, Zamani P, Abureden S, Chen Z (2014) Morphology and composition controlled platinum-cobalt alloy nanowires prepared by electrospinning as oxygen reduction catalyst. Nano Energy 10:135–143
5. Shao Y, Liu J, Wang Y, Lin Y (2009) Novel catalyst support materials for PEM fuel cells: current status and future prospects. J Mater Chem 19:46–59
6. Hoque MA, Hassan FM, Higgins D, Choi JY, Pritzker M, Knights S, Ye S, Chen Z (2014) Multigrain platinum nanowires consisting of oriented nanoparticles anchored on sulfur-doped graphene as a highly active and durable oxygen reduction electrocatalyst. Adv Mater 27:1229–1234
7. Higgins DC, Chen Z (2013) Recent progress in non-precious metal catalysts for PEM fuel cell applications. Can J Chem Eng 91:1881–1895
8. Chen Z, Higgins D, Yu A, Zhang L, Zhang J (2011) A review on non-precious metal electrocatalysts for PEM fuel cells. Energy Environ Sci 4:3167–3192
9. Jaouen F, Proietti E, Lefèvre M, Chenitz R, Dodelet JP, Wu G, Chung HT, Johnston CM, Zelenay P (2010) Recent advances in non-precious metal catalysis for oxygen-reduction reaction in polymer electrolyte fuel cells. Energ Environ Sci 4:114–130
10. Wu G, Zelenay P (2013) Nanostructured nonprecious metal catalysts for oxygen reduction reaction. Acc Chem Res 46:1878–1889
11. Jaouen F, Herranz J, Lefèvre M, Dodelet JP, Kramm UI, Herrmann I, Bogdanoff P, Maruyama J, Nagaoka T, Garsuch A, Dahn JR, Olson T, Pylypenko S, Atanassov P, Ustinov EA (2009) Cross-laboratory experimental study of non-noble-metal electrocatalysts for the oxygen reduction reaction. ACS Appl Mater Interfaces 1:1623–1639
12. Kramm UI, Lefèvre M, Larouche N, Schmeisser D, Dodelet J-P (2013) Correlations between mass activity and physicochemical properties of Fe/N/C Catalysts for the ORR in PEM fuel cell via Fe Mössbauer spectroscopy and other techniques. J Am Chem Soc 136:978–985
13. Lefevre M, Proietti E, Jaouen F, Dodelet JP (2009) Iron-based catalysts with improved oxygen reduction activity in polymer electrolyte fuel cells. Science 324:71–74
14. Proietti E, Jaouen F, Lefevre M, Larouche N, Tian J, Herranz J, Dodelet JP (2011) Iron-based cathode catalyst with enhanced power density in polymer electrolyte membrane fuel cells. Nat Commun 2:416
15. Wu G, More KL, Johnston CM, Zelenay P (2011) High-performance electrocatalysts for oxygen reduction derived from polyaniline, iron, and cobalt. Science 332:443–447
16. Zhao D, Shui JL, Grabstanowicz LR, Chen C, Commet SM, Xu T, Lu J, Liu DJ (2014) Highly efficient non-precious metal electrocatalysts prepared from one-pot synthesized zeolitic imidazolate frameworks. Adv Mater 26:1093–1097
17. Choi J, Hsu R, Chen Z (2010) Highly active porous carbon-supported nonprecious metal-N electrocatalyst for oxygen reduction reaction in PEM fuel cells. J Phys Chem C 114:8048–8053
18. Serov A, Artyushkova K, Atanassov P (2014) Fe-N-C oxygen reduction fuel cell catalyst derived from carbendazim: synthesis, structure, and reactivity. Adv Energy Mater 4:1301735
19. Zitolo A, Goellner V, Armel V, Sougrati MT, Mineva T, Stievano L, Fonda E, Jaouen F (2015) Identification of catalytic sites for oxygen reduction in iron- and nitrogen-doped graphene materials. Nat Mater 14:937–942
20. U. S. Drive (2013) Fuel cell technical team roadmap. http://energy.gov/sites/prod/files/2014/02/f8/fctt_roadmap_june2013.pdf
21. U.S. Department of Energy's 2014 Annual Merit Review and Peer Evaluation Meeting Presentation (2014) Non-precious metal fuel cell cathodes: catalyst development and electrode structure design. http://www.hydrogen.energy.gov/pdfs/review14/fc107_zelenay_2014_o.pdf
22. Jahnke H, Schoenborn M, Zimmermann G Electrochem Soc 303–318
23. Biddinger EJ, von Deak D, Ozkan US (2009) Nitrogen-containing carbon nanostructures as oxygen-reduction catalysts. Top Catal 52:1566–1574
24. Mamtani K, Ozkan US (2015) Heteroatom-doped carbon nanostructures as oxygen reduction reaction catalysts in acidic media: an overview. Catal Lett 145:436–450

25. Tylus U, Jia Q, Strickland K, Ramaswamy N, Serov A, Atanassov P, Mukerjee S (2014) Elucidating oxygen reduction active sites in pyrolyzed metal–nitrogen coordinated non-precious-metal electrocatalyst systems. J Phys Chem C 118:8999–9008
26. Ramaswamy N, Tylus U, Jia Q, Mukerjee S (2013) Activity descriptor identification for oxygen reduction on nonprecious electrocatalysts: linking surface science to coordination chemistry. J Am Chem Soc 135:15443–15449
27. Nallathambi V, Lee JW, Kumaraguru SP, Wu G, Popov BN (2008) Development of high performance carbon composite catalyst for oxygen reduction reaction in PEM proton exchange membrane fuel cells. J Power Sources 183:34–42
28. Olson TS, Pylypenko S, Fulghum JE, Atanassov P (2010) Bifunctional oxygen reduction reaction mechanism on non-platinum catalysts derived from pyrolyzed porphyrins. J Electrochem Soc 157:B54–B63
29. Serov A, Tylus U, Artyushkova K, Mukerjee S, Atanassov P (2014) Mechanistic studies of oxygen reduction on Fe-PEI derived non-PGM electrocatalysts. Appl Catal B 150–151:179–186
30. Hudak NS, Gallaway JW, Barton SC (2009) Mediated biocatalytic cathodes operating on gas-phase air and oxygen in fuel cells. J Electrochem Soc 156:B9–B15
31. Parvez K, Yang S, Hernandez Y, Winter A, Turchanin A, Feng X, Müllen K (2012) Nitrogen-doped graphene and its iron-based composite as efficient electrocatalysts for oxygen reduction reaction. ACS Nano 6:9541–9550
32. Matter PH, Wang E, Arias M, Biddinger EJ, Ozkan US (2006) Oxygen reduction reaction catalysts prepared from acetonitrile pyrolysis over alumina-supported metal particles. J Phys Chem B 110:18374–18384
33. Matter PH, Zhang L, Ozkan US (2006) The role of nanostructure in nitrogen-containing carbon catalysts for the oxygen reduction reaction. J Catal 239:83–96
34. Garsuch A, MacIntyre K, Michaud X, Stevens DA, Dahn JR (2008) Fuel cell studies on a non-noble metal catalyst prepared by a template-assisted synthesis route. J Electrochem Soc 15:B953–B957
35. Kim JH, Ishihara A, Mitsushima S, Kamiya N, Ota KI (2007) Catalytic activity of titanium oxide for oxygen reduction reaction as a non-platinum catalyst for PEFC. Electrochim Acta 52:2492–2497
36. Maldonado S, Stevenson KJ (2005) Influence of nitrogen doping on oxygen reduction electrocatalysis at carbon nanofiber electrodes. J Phys Chem B 109:4707–4716
37. Chung HT, Won JH, Zelenay P (2013) Active and stable carbon nanotube/nanoparticle composite electrocatalyst for oxygen reduction. Nat Commun 4:1922
38. Wu G, Johnston CM, More KL, Mack NH, Artyushkova K, Ferrandon M, Nelson M, Pacheco JSL, Conradson SD, More KL, Myers DJ, Zelenay P (2011) Synthesis-structure-performance correlation for polyaniline–Me–C non-precious metal cathode catalysts for oxygen reduction in fuel cells. J Mater Chem 21:11392–11405
39. Jaouen F, Herranz J, Lefèvre M, Dodelet JP, Kramm UI, Herrmann I, Bogdanoff P, Maruyama J, Nagaoka T, Garsuch A, Dahn JR, Olson T, Pylypenko S, Atanassov P, Ustinov EA (2009) Cross-laboratory experimental study of non-noble-metal electrocatalysts for the oxygen reduction reaction. ACS Appl Mater Interfaces 1:1623–1639
40. Wu G, Chen Z, Artyushkova K, Garzon FH, Zelenay P (2009) Polyaniline-derived non-precious catalyst for the polymer electrolyte fuel cell cathode. ECS Trans 16:159–170
41. Wu G, Artyushkova K, Ferrandon M, Kropf AJ, Myers DJ, Zelenay P (2009) Performance durability of polyaniline-derived non-precious cathode catalysts. ECS Trans 25:1299–1311
42. Wu G, Mack NH, Gao W, Ma S, Zhong R, Han J, Baldwin JK, Zelenay P (2012) Nitrogen-doped graphene-rich catalysts derived from heteroatom polymers for oxygen reduction in nonaqueous lithium–O2 battery cathodes. ACS Nano 6:9764–9776
43. Bezerra CWB, Zhang L, Liu H, Lee K, Marques ALB, Marques EP, Wang H, Zhang J (2007) A review of heat-treatment effects on activity and stability of PEM fuel cell catalysts for oxygen reduction reaction. J Power Sources 173:891–908

44. Bezerra CWB, Zhang L, Lee K, Liu H, Marques AL, Marques EP, Wang H, Zhang J (2008) A review of Fe–N/C and Co–N/C catalysts for the oxygen reduction reaction. Electrochim Acta (53):4937–4951
45. Ohms D, Herzog S, Franke R, Neumann V, Wiesener K, Gamburcev S, Kaisheva A, Liev L (1992) Influence of metal ions on the electrocatalytic oxygen reduction of carbon materials prepared from pyrolyzed polyacrylonitrile. J Power Sources 38:327–334
46. Peng H, Liu F, Liu X, Liao S, You C, Tian X, Nan H, Luo F, Song H, Fu Z, Huang P (2014) Effect of transition metals on the structure and performance of the doped carbon catalysts derived from polyaniline and melamine for ORR application. ACS Catal 4:3797–3805
47. Chung HT, Zelenay P (2015) A simple synthesis of nitrogen-doped carbon micro- and nanotubes. Chem Commun 51:13546–13549
48. Li Q, Wu G, Cullen DA, More KL, Mack NH, Chung HT, Zelenay P (2014) Phosphate-tolerant oxygen reduction catalysts. ACS Catal 4:3193–3200
49. Wu G, More KL, Xu P, Wang HL, Ferrandon M, Kropf AJ, Myers DJ, Ma S, Johnston CM, Zelenay P (2013) Carbon-nanotube-supported graphene-rich non-precious metal oxygen reduction catalyst with enhanced performance durability. Chem Commun 49:3291–3293
50. Wu G, Chen Y-S, Xu B-Q (2005) Remarkable support effect of SWNTs in Pt catalyst for methanol electrooxidation. Electrochem Commun 7:1237–1243
51. Wu G, Xu B-Q (2007) Carbon nanotube supported Pt electrodes for methanol oxidation: A comparison between multi-and single-walled carbon nanotubes. J Power Sources 174:148–158
52. Ferrari AC, Robertson J (2000) Interpretation of Raman spectra of disordered and amorphous carbon. Phys Rev B 61:14095–14107
53. Tuinstra F, Koenig JL (1970) Raman spectrum of graphite. J Chem Phys 53:1126–1130
54. Ferrandon M, Kropf AJ, Myers DJ, Artyushkova K, Kramm U, Bogdanoff P, Wu G, Johnston CM, Zelenay P (2012) Multitechnique characterization of a polyaniline–iron–carbon oxygen reduction catalyst. J Phys Chem C 116:16001–16013
55. Kramm U, Wurmbach IA, Geppert H, Radnik J, Fiechter S, Bogdanoff P (2011) Influence of the electron-density of FeN-centers towards the catalytic activity of pyrolyzed FeTMPPCl-based ORR-electrocatalysts. J Electrochem Soc 158:B69–B78
56. Herranz J, Jaouen F, Lefevre M, Kramm UI, Proietti E, Dodelet JP, Bogdanoff P, Fiechter S, Wurmbach IA, Bertrand P, Arruda TM, Mukerjee S (2011) Unveiling N-protonation and anion-binding effects on Fe/N/C catalysts for O_2 reduction in proton-exchange-membrane fuel cells. J Phys Chem C 115:16087–16097
57. Kramm UI, Herranz J, Larouche N, Arruda TM, Lefevre M, Jaouen F, Bogdanoff P, Fiechter S, Wurmbach IA, Mukerjee S, Dodelet JP (2012) Structure of the catalytic sites in Fe/N/C-catalysts for O_2-reduction in PEM fuel cells. Phys Chem Chem Phys 14:11673–11688
58. Matter PH, Wang E, Arias M, Biddinger EJ, Ozkan US (2007) Oxygen reduction reaction activity and surface properties of nanostructured nitrogen-containing carbon. J Mol Catal A Chem 264:73–81
59. Matter PH, Wang E, Millet JMM, Ozkan US (2007) Characterization of the iron phase in CN_x-based oxygen reduction reaction catalysts. J Phys Chem C 111:1444–1450
60. Liu G, Li XG, Ganesan P, Popov BN (2009) Development of non-precious metal oxygen-reduction catalysts for PEM fuel cells based on N-doped ordered porous carbon. Appl Catal B 93:156–165
61. Jaouen F, Lefevre M, Dodelet JP, Cai M (2006) Heat-treated Fe/N/C catalysts for O_2 electroreduction: Are active sites hosted in micropores? J Phys Chem B 110:5553–5558
62. Jaouen F, Marcotte S, Dodelet JP, Lindbergh G (2003) Oxygen reduction catalysts for polymer electrolyte fuel cells from the pyrolysis of iron acetate adsorbed on various carbon supports. J Phys Chem B 107:1376–1386
63. Li W, Yu A, Higgins DC, Llanos BG, Chen Z (2010) Biologically inspired highly durable iron phthalocyanine catalysts for oxygen reduction reaction in polymer electrolyte membrane fuel cells. J Am Chem Soc 132:17056–17058
64. Zagal JH, Griveau S, Silva F, Nyokong T, Bedioui F (1992) Metallophthalocyanines as catalysts in electrochemical reactions. Coord Chem Rev 119:89–136

65. Higgins D, Chen Z (2013) Electrocatalysis in fuel cells. In: Shao M (ed) Lecture Notes in Energy Ch. 9, vol 9. Springer, London, pp 247–269
66. Serov A, Robson MH, Artyushkova K, Atanassov P (2012) Templated non-PGM cathode catalysts derived from iron and poly(ethyleneimine) precursors. Appl Catal B 127:300–306
67. Robson MH, Serov A, Artyushkova K, Atanassov P (2013) A mechanistic study of 4-aminoantipyrine and iron derived non-platinum group metal catalyst on the oxygen reduction reaction. Electrochim Acta 90:656–665
68. Serov A, Robson MH, Smolnik M, Atanassov P (2012) Templated bi-metallic non-PGM catalysts for oxygen reduction. Electrochim Acta 80:213–218
69. Ma S, Goenaga GA, Call AV, Liu D-J (2011) Cobalt imidazolate framework as precursor for oxygen reduction reaction electrocatalysts. Chem Eur J 17:2063–2067
70. Zamani P, Higgins D, Hassan F, Jiang G, Wu J, Abureden S, Chen Z (2014) Electrospun iron–polyaniline-polyacrylonitrile derived nanofibers as non-precious oxygen reduction reaction catalysts for PEM fuel cells. Electrochim Acta 139:111–116
71. Chung HT, Johnston CM, Artyushkova K, Ferrandon M, Myers DJ, Zelenay P (2010) Cyanamide-derived non-precious metal catalyst for oxygen reduction. Electrochem Commun 12:1792–1795

http://www.springer.com/978-3-319-31170-8

Electrochemistry of N4 Macrocyclic Metal Complexes
Volume 1: Energy
Zagal, J.H.; Bedioui, F. (Eds.)
2016, XV, 316 p. 164 illus., 116 illus. in color.,
Hardcover
ISBN: 978-3-319-31170-8